THE GLOBAL STABILITY ANALYSIS OF LAMINAR SEPARATION FLOW OVER AN AIRFOIL

Asei TEZUKA*, Kojiro SUZUKI* and Kenichi RINOIE*
***Department of Aeronautics &Astronautics, University of Tokyo, 113-8656, Japan**

Keywords: *Stability Analysis, Incompressible Flow, Numerical Analysis*

Abstract

In this paper, the stability of non-parallel flowfield has been investigated by applying the global stability analysis. Chiba's method, which is a method for the global stability analysis, is modified in order to increase the efficiency of the calculation and to calculate the stability of an arbitrary domain of the flowfield. The modified method was applied for the laminar flowfield around a NACA0012 airfoil. We focus on the domain which is over the leeside of the airfoil. Oscillatory modes of the domain were numerically calculated using the modified method. The period and the wavelength of the most amplified mode were compared with the result of the local stability analysis incorporating Kelvin-Helmholtz instability. The results of our study agree with those of the local stability analysis.

1 Introduction

The flow around a wing demonstrates various oscillatory phenomena, for example, Karman vortex which is observed at wake region, and Kelvin-Helmholtz instability which is observed in the laminar separation bubble. Such oscillatory phenomena were explained by the results of the local stability analysis. However, to study the stability of a general flowfield, in other words, the stability of a non-parallel flowfield, other approach is needed.

The stability of flow around a various shaped body can be analyzed using the application of the global stability analysis. In the global stability analysis, the unstable distribution of the velocity perturbation, which is known as "mode", is calculated. Natarajan[1] examined the global stability of the flow around a sphere and explained the mechanism of the transition from steady axisymmetric flow to steady non-axisymmetric flow. In this paper, the term "transition" stands for such a change of flowfield in laminar flow. This phenomenon is different from the transition from laminar flow to turbulent flow.

In the case for a flow around a sphere, a steady non-axisymmetric flow is observed when the Reynolds number is between 210 and 270. The critical Reynolds number from steady flow to oscillatory is obtained as Re=270. However, the critical Reynolds number from non-oscillatory axisymmetric flow to non-oscillatory symmetric flow is also obtained. This critical Reynolds number is 210. Since this value is lower than the critical Reynolds number for oscillatory flow, non-oscillatory non-axisymmetric flow is observed.

In the author's previous study, the global stability of flow around an ellipsoid[2] and a blunt cylinder[3] at angles of attack was investigated. To calculate the global stability of the flowfield, Chiba's method[4] was used, because it can be easily coupled with the Navier-Stokes analysis using the finite-difference method on the generalized coordinates. A characteristic of Chiba's method is that several sets of velocity disturbances are added to the numerical result of Navier-Stokes equations which becomes the initial conditions used to calculate the Navier-Stokes equations. The stability of flow is estimated whether the velocity disturbances are magnified or not. Three-dimensional flow around a sphere was analyzed to check the validity of the numerical code used. The results were in good agreement with the results of Natarajan[1].

In the case of the flow around above-mentioned configurations, the region of flowfield which is transformed by the appearance of transitional mode is limited only in the wake region of the body. Calculating the stability of flow by adding a disturbance velocity to the whole computational domain is considered as inefficient. If we calculate only the region of flowfield which is supposed to be significant for the stability of flowfield, the efficiency of calculation will be improved[5].

The governing equation of the modified method is obtained analytically by the perturbation expansion of the Navier-Stokes equations. Using this modified method and calculating a certain region of flowfield, the computational time becomes shorter than the Chiba's method.

In this study, the flow over a two-dimensional NACA0012 airfoil at angle of attack is analyzed using the modified stability analysis. The laminar separation and subsequent transition to turbulent flow over the airfoil plays an important role for the flow around the airfoil, especially at a high angle of attack and for airfoil stall. Although numerous researches have been conducted, precise predictions of separation and transition to turbulent flow over the airfoil have not been accomplished[6].

The main purpose of this paper is to apply the modified global stability analysis to the laminar separation flow over the airfoil. Stability analysis is considered as a promising approach to clarify the mechanism of the onset of transition to turbulent flow observed in the separated flow over the airfoil. The Reynolds number based on the chord length is set as $Re = 1.0 \times 10^5$. From the result of our numerical simulation, it is verified that a sequence of vortex is generated on the airfoil and these vortices are convected to leeward. This phenomenon is considered to be caused by the Kelvin-Helmholtz instability. Therefore, our result of stability analysis is compared with the result of Kelvin-Helmholtz instability. To investigate the effect of the Reynolds number, the stability of flow in a different Reynolds number of 2.0×10^5 was also calculated.

2. Numerical Method

2.1 Global Stability Analysis

The incompressible laminar Navier-Stokes equations are written as follows:

$$\partial \boldsymbol{u} / \partial t = \boldsymbol{f}(\boldsymbol{u}), \tag{1}$$

where the vector $\boldsymbol{u}$ is the column of the velocity components at all the computational nodes.

$$\boldsymbol{u} = (u_{1,1}\ v_{1,1} \cdots u_{i_{\max}, j_{\max}}\ v_{i_{\max}, j_{\max}})^T,$$

If the number of computational nodes ($i_{\max} \times j_{\max}$) is N, the dimension of $\boldsymbol{u}$ becomes $2N$ in the two-dimensional case. Pressure is not included in the dependent variables, since it is calculated from the velocity. A Taylor series expansion is applied to Eq. (1) around the stationary solution $\boldsymbol{u}_0$:

$$\boldsymbol{f}(\boldsymbol{u}_0 + \tilde{\boldsymbol{u}}) = \boldsymbol{f}(\boldsymbol{u}_0) + \frac{\partial \boldsymbol{f}(\boldsymbol{u}_0)}{\partial \boldsymbol{u}} \tilde{\boldsymbol{u}} + O(\tilde{\boldsymbol{u}}^2), \tag{2}$$

where $\tilde{\boldsymbol{u}}$ is a small disturbance. Considering that the second or higher order terms with respect to $|\tilde{\boldsymbol{u}}|$ are negligibly small, the linearized stability equation is given as:

$$\frac{\partial \tilde{\boldsymbol{u}}}{\partial t} = \frac{\partial \boldsymbol{f}(\boldsymbol{u}_0)}{\partial \boldsymbol{u}} \tilde{\boldsymbol{u}} \equiv \boldsymbol{A} \tilde{\boldsymbol{u}}, \tag{3}$$

where $\boldsymbol{A} \equiv \partial \boldsymbol{f}(\boldsymbol{u}_0) / \partial \boldsymbol{u}$ is the Jacobian matrix.

Substituting the eigenvalue λ and eigenvector $\boldsymbol{\phi}$ of matrix A into Eq.(3), we obtain

$$\partial \boldsymbol{\phi} / \partial t = \lambda \boldsymbol{\phi}.$$

We can evaluate the stability of flow by the real part of λ (i.e. $\Re(\lambda)$). The mode of velocity disturbance is represented by $\boldsymbol{\phi}$. When the real part of the eigenvalue is positive or negative, the magnitude of the mode is growing (the flow is unstable) or diminishing (the flow is stable), respectively. The period of the oscillatory mode is evaluated by the imaginary part of λ (i.e. $\Im(\lambda)$). The imaginary part represents the frequency of the oscillation. When the imaginary part of the eigenvalue is zero or non-

zero, the mode is steady or oscillatory, respectively.

2.2 Application of the Approximate Eigensystem Analysis

2.2.1 Approximate Eigensystem Analysis

The global stability is analyzed by the eigensystem analysis of Eq.(3). However, the size of matrix $\boldsymbol{A}$ is $2N \times 2N$. It is inefficient to calculate the eigensystem of matrix $\boldsymbol{A}$ directly. Chiba[4] adapted Eriksson's method[7] to determine the critical Reynolds number in the case of a circular cylinder and obtained reasonable results. In his approach, Arnoldi's method[8] was used to calculate the eigenvalue approximately.

Integrating Eq.(3) with respect to time from 0 to T gives:

$$\tilde{\boldsymbol{u}}(T) = \exp(A\,T)\tilde{\boldsymbol{u}}(0)\,, \tag{4}$$

The approximate eigensystem of $\boldsymbol{B}(\equiv \exp(\boldsymbol{A}\,T))$ is numerically calculated by Arnoldi's method.

Suppose the approximate eigensystem of matrix $\boldsymbol{B}$ is expressed by the vector which is contained in the Krylov subspace

$$K_M = \mathrm{span}\{\boldsymbol{\zeta}_1, \boldsymbol{B}\boldsymbol{\zeta}_1, ..., \boldsymbol{B}^{M-1}\boldsymbol{\zeta}_1\}\,.$$

The normalized orthogonal basis vectors of subspace K_M which are written as $\boldsymbol{\zeta}_i$ ($1 \le i \le M$, $M \ll N$) are introduced. $\boldsymbol{\zeta}_i$ is a column vector and the number of elements are $2N$. The vector $\boldsymbol{\zeta}_1$ is given by random numbers. To obtain the basis vector $\boldsymbol{\zeta}_i$ ($2 \le i \le M$), the Gram-Schmidt orthogonalization method is used. Suppose that $\boldsymbol{B}\boldsymbol{\zeta}_1$ is calculated, then $\boldsymbol{\zeta}_2$ is defined by the orthogonality condition. The vector $\boldsymbol{\zeta}_2$ is introduced to describe the vector $\boldsymbol{B}\boldsymbol{\zeta}_1$ by using a set of orthonormal basis $\boldsymbol{\zeta}_1$ and $\boldsymbol{\zeta}_2$:

$$\boldsymbol{B}\boldsymbol{\zeta}_1 = c_{1,1}\boldsymbol{\zeta}_1 + c_{2,1}\boldsymbol{\zeta}_2\,. \tag{5}$$

The procedure of the Chiba's method to calculate $\boldsymbol{B}\boldsymbol{\zeta}_1$ is expressed in section 2.2.2.

The vectors, $\boldsymbol{\zeta}_3$, $\boldsymbol{\zeta}_4$, ..., $\boldsymbol{\zeta}_M$ are calculated in the same way: First, calculates the vector $\boldsymbol{B}\boldsymbol{\zeta}_i$. Then, the vector $\boldsymbol{\zeta}_{i+1}$ is introduced as:

$$\boldsymbol{B}\boldsymbol{\zeta}_i = c_{1,i}\boldsymbol{\zeta}_1 + c_{2,i}\boldsymbol{\zeta}_2 + \cdots + c_{j,i}\boldsymbol{\zeta}_j + \cdots + c_{i+1,i}\boldsymbol{\zeta}_{i+1}\,. \tag{6}$$

Gram-Schmidt orthogonalization was applied to calculate $\boldsymbol{\zeta}_{i+1}$. The coefficient $c_{j,i}$ of orthonormal basis $\boldsymbol{\zeta}_j$ ($1 \le j \le i$) is calculated as:

$$c_{j,i} = \boldsymbol{B}\boldsymbol{\zeta}_i \cdot \boldsymbol{\zeta}_j\,. \tag{7}$$

Then, $c_{i+1,i}\boldsymbol{\zeta}_{i+1}$ is calculated from the following relation:

$$c_{i+1,i}\boldsymbol{\zeta}_{i+1} = \boldsymbol{B}\boldsymbol{\zeta}_i - (c_{1,i}\boldsymbol{\zeta}_1 + c_{2,i}\boldsymbol{\zeta}_2 + \cdots + c_{i,i}\boldsymbol{\zeta}_i)\,. \tag{8}$$

At the end of the calculation, the following equation is obtained

$$\begin{aligned}\boldsymbol{B}\boldsymbol{\zeta}_M = {} & c_{1,M}\boldsymbol{\zeta}_1 + c_{2,M}\boldsymbol{\zeta}_2 + \cdots + c_{j,M}\boldsymbol{\zeta}_j + \cdots \\ & + c_{M,M}\boldsymbol{\zeta}_M + c_{M+1,M}\boldsymbol{\zeta}_{M+1}\end{aligned}\,. \tag{9}$$

In the case that M is large and $|\,c_{M+1,M}\boldsymbol{\zeta}_{M+1}\,|$ is small, we can approximate Eq.(9) as

$$\begin{aligned}\boldsymbol{B}\boldsymbol{\zeta}_M = {} & c_{1,M}\boldsymbol{\zeta}_1 + c_{2,M}\boldsymbol{\zeta}_2 + \cdots \\ & + c_{j,M}\boldsymbol{\zeta}_j + \cdots + c_{M,M}\boldsymbol{\zeta}_M\end{aligned}\,. \tag{10}$$

The coefficient $c_{j,k}$ and basis vector $\boldsymbol{\zeta}_j$ satisfy

$$\boldsymbol{B}\{\boldsymbol{\zeta}_1, ..., \boldsymbol{\zeta}_M\} = \{\boldsymbol{\zeta}_1, ..., \boldsymbol{\zeta}_M\} \times \underbrace{\begin{bmatrix} c_{1,1} & \cdots & \cdots & c_{1,M-1} & c_{1,M} \\ c_{2,1} & \cdots & \cdots & c_{2,M-1} & c_{1,M} \\ 0 & \ddots & & \vdots & \vdots \\ \vdots & \ddots & \ddots & \vdots & \vdots \\ 0 & \cdots & 0 & c_{M,M-1} & c_{M,M} \end{bmatrix}}_{\boldsymbol{H}}\,. \tag{11}$$

The $M \times M$ matrix $\boldsymbol{H}$ whose elements are $c_{j,k}$ is obtained. The eigensystem of $\boldsymbol{B}$ is approximately calculated from the eigensystem analysis of the matrix $\boldsymbol{H}$ of size $M \times M$ instead of the matrix $\boldsymbol{B}$ of size $2N \times 2N$. The eigenvalue $\lambda^{(H)}$ and eigenvector $\boldsymbol{\psi}^{(H)}$ of matrix $\boldsymbol{H}$ satisfies the equation:

$$\boldsymbol{H}\boldsymbol{\psi}^{(H)} = \lambda^{(H)}\boldsymbol{\psi}^{(H)}\,.$$

Then, the Eq.(11) becomes

$$\begin{aligned} \boldsymbol{B}\{\zeta_1,...,\zeta_M\}\psi^{(H)} &= \{\zeta_1,...,\zeta_M\}\boldsymbol{H}\psi^{(H)} \\ &= \{\zeta_1,...,\zeta_M\}\lambda^{(H)}\psi^{(H)} \\ &= \lambda^{(H)}\{\zeta_1,...,\zeta_M\}\psi^{(H)} . \end{aligned} \quad (12)$$

Therefore the eigenvalue $\lambda^{(H)}$ of matrix $\boldsymbol{H}$ is an approximate eigenvalue of matrix $\boldsymbol{B}$. The vector $\{\zeta_1,...,\zeta_M\}\psi^{(H)}$ becomes the approximate eigenvector of matrix $\boldsymbol{B}$. The approximate eigenvalue $\lambda^{(B)}$ and eigenvector $\phi^{(B)}$ of matrix $\boldsymbol{B}$ is calculated from the Eq.(13)(14).

$$\lambda^{(B)} = \lambda^{(H)}, \quad (13)$$

$$\phi^{(B)} = \{\zeta_1,...,\zeta_M\}\psi^{(H)} . \quad (14)$$

The eigenvalue $\lambda^{(A)}$ of the matrix $\boldsymbol{A}$ is obtained by the relation:

$$\lambda^{(B)} = \exp(\lambda^{(A)}T) . \quad (15)$$

The eigenvector $\phi^{(A)}$ for the system $\boldsymbol{A}$ is the same as that for the system $\boldsymbol{B}$.

$$\phi^{(A)} = \phi^{(B)} . \quad (16)$$

It should be noted that in this method, less stable mode with larger real part of the eigenvalue is computed more accurately. The transition of flow from a state to another state is caused by the mode that has the largest real part of eigenvalue. So by using the approximate eigensystem analysis, the mode which dominate the transition is obtained efficiently.

2.2.2 Calculation of $B\zeta_i$ by Chiba's method

From the relation of Eq.(2), we can say that $\tilde{\boldsymbol{u}}(0)$ is a vector disturbance at $t=0$, and $\tilde{\boldsymbol{u}}(T)$ is a vector disturbance at $t=T$. In Chiba's method, the Navier-Stokes equations are solved from $t=0$ to $t=T$ using such initial value that contains the velocity disturbance. Two types of initial values: $\boldsymbol{u}_{i+}{}^{(\mathrm{ini})}(\equiv \boldsymbol{u}_0 + \varepsilon\zeta_1)$ and $\boldsymbol{u}_{i-}{}^{(\mathrm{ini})}(\equiv \boldsymbol{u}_0 - \varepsilon\zeta_1)$ are introduced. $\boldsymbol{u}_0$ is the converged solution of the Navier-Stokes equations which is considered as a basic flow of the stability analysis.

In order to calculate $\boldsymbol{B}\zeta_1$, the Navier-Stokes equations are solved using $\boldsymbol{u}_{i+}{}^{(\mathrm{ini})}$ and $\boldsymbol{u}_{i-}{}^{(\mathrm{ini})}$ as an initial value. The result at $t=T$ are written as $\boldsymbol{u}_{i+}{}^{(\mathrm{fin})}$ and $\boldsymbol{u}_{i-}{}^{(\mathrm{fin})}$, respectively. Then $\boldsymbol{B}\zeta_1$ is obtained as:

$$\boldsymbol{B}\zeta_1 = (\boldsymbol{u}_{1+}{}^{(\mathrm{fin})} - \boldsymbol{u}_{1-}{}^{(\mathrm{fin})})/2\varepsilon . \quad (17)$$

The vector ζ_i, whose number of elements are $2N$, should satisfy the normalized condition $|\zeta_i| = 1$. Then, the component of ζ_i becomes small if the number of elements $2N$ is large. For N is the number of gridpont, the magnitude of ζ_i depends on the size of computational mesh. Therefore, to control the magnitude of the initial disturbance, the parameter ε is introduced.

2.3 Derivation of the Linearized Perturbation Equations

In MAC method[9], which is a numerical method for incompressible Navier-Stokes equations, the Navier-Stokes equations (18), (19) and a Poisson's equation (20) are derived.

$$u_t + uu_x + vu_y = -p_x + (u_{xx} + u_{yy})/Re \quad (18)$$

$$v_t + uv_x + vv_y = -p_y + (v_{xx} + v_{yy})/Re \quad (19)$$

$$\begin{aligned} p_{xx} + p_{yy} = &-u_x{}^2 - 2u_y v_x - v_y{}^2 \\ &+(u_x + v_y)/\Delta t \end{aligned} \quad (20)$$

These equations are coupled and solved numerically.

In this study, first-order perturbation of Eq.(18)-(20) are introduced to calculate $\tilde{\boldsymbol{u}}(T)$. Let U, V and P be the converged steady solution of Navier-Stokes equations which was considered as base flow. Substituting U, V and P into Eq.(18)-(20) gives:

$$UU_x + VU_y = -P_x + (U_{xx} + U_{yy})/Re \quad (21)$$

$$UV_x + VV_y = -P_y + (U_{xx} + V_{yy})/Re \quad (22)$$

$$\begin{aligned} P_{xx} + P_{yy} = &-U_x{}^2 - 2U_y V_x - V_y{}^2 \\ &+(U_x + V_y)/\Delta t \end{aligned} \quad (23)$$

Substituting $U+u'$, $V+v'$ and $P+p'$ into Eq.(18)-(20), yields:

$$(U+u')_t+(U+u')(U+u')_x+(V+v')(U+u')_y = -(P+p')_x+((U+u')_{xx}+(U+u')_{yy})/Re \quad (24)$$

$$(V+v')_t+(U+u')(V+v')_x+(V+v')(V+v')_y = -(P+p')_y+((V+v')_{xx}+(V+v')_{yy})/Re \quad (25)$$

$$(P+p)_{xx}+(P+p)_{yy} = -(U+u)_x^2-2(U+u)_y(V+v)_x-(V+v)_y^2 + ((U+u)_x+(V+v)_y)/\Delta t \quad (26)$$

Calculating the difference between Eqs.(21)-(23) and Eqs.(24)-(26), and neglecting the higher order term of the perturbation, we get the linearlized perturbation equation:

$$p'_{xx}+p'_{yy} = -2\,U_x\,u'_x-2u'_yV_x-2U_yv'_x-2\,v'_yV_y+(u'_x+v'_y)/\Delta t \quad (27)$$

$$u'_t+u'U_x+Uu'_x+v'U_y+Vu'_y = -p'_x+(u'_{xx}+u'_{yy})/Re \quad (28)$$

$$v'_t+u'V_x+Uv'_x+v'V_y+Vv'_y = -p'_y+(v'_{xx}+v'_{yy})/Re \quad (29)$$

The velocity perturbation at time T is calculated by the time marching of Eqs. (27)-(29). If the initial disturbances, $u'(0)$ and $v'(0)$, are given, $u'(T)$ and $v'(T)$ which are the disturbances at time T is calculated by Eqs. (27)-(29). Then the eigensystem of matrix B is calculated by using the Arnoldi's method. This approach reduces the computational time almost by half comparing to the Chiba's method. This is because the Chiba's method requires twice calculation for Eqs.(18)-(20) to get $\tilde{\boldsymbol{u}}(T)$. In the first calculation, the initial condition of Navier-Stokes equation is $\boldsymbol{u}_0+\varepsilon\tilde{\boldsymbol{u}}(0)$ and then $\boldsymbol{u}_0-\varepsilon\tilde{\boldsymbol{u}}(0)$ becomes the initial condition. If we use the perturbation equations (27)-(29), $\tilde{\boldsymbol{u}}(T)$ is obtained by single calculation. Therefore the computational cost for the calculation of the stability is reduced by using the perturbation equation.

2.3 Numerical scheme for linearized perturbation equation

The central difference was applied for the discretization of the equation except the convection term. If we discrete the convection term by central difference, numerical oscillation may diverge and we may not calculate the flow. Therefore, upwind difference is applied to the convection term for the numerical simulation of the flow. In this study, third-order upwind difference[10] was applied to the convection term.

$$(u\,u_x)_i = u_i\frac{-u_{i+2}+8(u_{i+1}-u_{i-1})+u_{i-2}}{12\Delta x} + |u_i|\frac{u_{i+2}-4u_{i+1}+6u_i-4u_{i-1}+u_{i-2}}{12\Delta x} \quad (30)$$

To simplify the expression, the first term and the second term of the right-hand side which correspond to the first and the fourth derivative is expressed as $f_1(u_i)$ and $f_4(u_i)$, respectively. Then, Eq. (30) is simplified as:

$$(u\,u_x)_i = u_if_1(u_i)+|\,u_i\,|\,f_4(u_i) \quad (31)$$

The first term and the fourth term of the linearlized perturbation equation (28)

$$u'U_x+Uu'_x+v'U_y+Vu'_y, \quad (32)$$

correspond to the convection term of the numer ical computation. If we apply the upwind differ ence to the first and the second term of Eq.(32) (i.e. $u'U_x+Uu'_x$), we get

$$u'U_x+Uu'_x = u'_if_1(U_i)+|\,u'_i\,|\,f_4(U_i) + U_if_1(u'_i)+|\,U_i\,|\,f_4(u'_i) \quad (33)$$

However, the second term of the right-hand side calculates the absolute value of the perturbation u'_i. If u'_i and $-u'_i$ are substituted to Eq. (33), the value of the second term becomes the same. When the input of a linear system is a sign inversion of u'_i, the output should be a sign inversion. Hence, Eq.(33) is an incorrect method to solve the convection term of the linear perturbation equation. We have to make other method for Eq.(33). If the convection term is treated inadequately, the numerical divergence will be caused. The result of the stability analysis is affected by the scheme of the convection term. To check the influence of the numerical viscosity, three types

of scheme (A), (B) and (C) are introduced to discrete the convection term.

Scheme (A)

Scheme (A) is derived from an idea to solve the perturbation equations numerically. The first term of Eq. (32) implies that if the basic flow is accelerating or decelerating, the disturbances decay or amplify in the streamwise direction, respectively. Therefore, this term is considered not to cause numerical divergence. The perturbation equation may be calculated numerically if the numerical viscosity of this term is omitted. Then, the following equation is used in scheme (A).

$$u_i' f_1(U_i) + U_i f_1(u_i') + |U_i| f_4(u_i') \tag{34}$$

Scheme (B)

Scheme (B) is consistent with the Chiba's method which calculate the amplification of the disturbance by adding velocity disturbances to the basic flow and solving the Navier-Stokes equations using such initial conditions. Substituting U and P into Eq. (31) gives

$$U_i f_1(U_i) + |U_i| f_4(U_i), \tag{35}$$

and substituting $U + u'$ and $P + p'$ into Eq. (31) gives

$$(U_i + u_i') f_1(U_i + u_i') + |U_i + u_i'| f_4(U_i + u_i'). \tag{36}$$

Considering the limit of $u' \to 0$, the absolute value of the second term of Eq.(36) is defined by the sign of U.

If U is larger than zero:

$$(U_i + u_i') f_1(U_i + u_i') + (U_i + u_i') f_4(U_i + u_i'). \tag{37}$$

If U is smaller than zero:

$$(U_i + u_i') f_1(U_i + u_i') - (U_i + u_i') f_4(U_i + u_i'). \tag{38}$$

Calculating the difference of Eq.(35) and neglecting the second order terms gives

If U is larger than zero:

$$u_i' f_1(U_i) + U_i f_1(u_i') + u_i' f_4(U_i) + U_i f_4(u_i') \tag{39}$$

If U is smaller than zero:

$$u_i' f_1(U_i) + U_i f_1(u_i') - (u_i' f_4(U_i) + U_i f_4(u_i')) \tag{40}$$

Therefore, Eqs.(39)(40) are used by Scheme (B).

Scheme (C)

Scheme (C) has no numerical viscosity in the convection term.

if we neglect the third term of Eq.(34) which is a numerical viscosity of Uu_x', we get Eq.(41).

$$u_i' f_1(U_i) + U_i f_1(u_i') \tag{41}$$

In the case of a subcritical condition, physical damping is considered to be dominating when compared to the numerical instability. Then, the numerical divergence is suppressed by the physical damping. If this consideration is true, we can calculate the perturbation equation by Eq.(41) which has no numerical viscosity. Then, scheme (C) is derived. If the amplification factor and the distribution of the velocity disturbance is the same among the scheme (A), (B) and (C), the effect of the numerical viscosity is considered to be negligible. In our previous study[11], the stability of the flow around a circular cylinder was calculated and the result calculated by using scheme (A), (B) and (C) are compared. Those results are the same if the amplification factor of the mode is large. This result indicates that physical instability is dominating when compared to the numerical instability and the effect of the numerical viscosity is negligible. To calculate the convection term of the perturbation equation, the choice of the scheme dose not cause any problem. In this study, the scheme(A) is applied to solve the perturbation equation.

2.4 Computational Conditions

For accurate evaluation of the stability of the flow, M must be large enough. To investigate the onset of the oscillation, the mode which has a large amplification factor was focused on. The value $\Re(\lambda^{(A)})$ of such mode is large. According to the increase of M, the value of $\lambda^{(A)}$ converges if the real part of $\lambda^{(A)}$ is large. When M is 40, the dependency of M becomes very small. Therefore, M is set as 40.

If T is larger than the half period of oscillation, aliasing occurs and the period of

oscillation appears longer than the actual period. In this study, the order the magnitude of the frequency can be estimated by the result of numerical simulation. Then, T is set as 0.01.

The MAC method[9] was used to solve the Navier-Stokes equations. The Poisson's equation for pressure was solved by the SOR method. The Euler explicit scheme was used for time integration. The third-order upwind finite-difference[10] is applied for the convection term. The grid is C type around the body and the number of grid is 501 x 101. At the outer boundary, the free-stream boundary condition and zero-th order extrapolation are applied at the inflow and outflow boundary, respectively. The value of the velocity vector $\boldsymbol{u}$ at the inflow boundary is set as freestream condition and the value of the disturbance velocity vector $\tilde{\boldsymbol{u}}$ is set as zero.

3. Results

3.1 $Re = 1.0 \times 10^5$ Case

The flow around a NACA0012 airfoil was numerically calculated. The Reynolds number was 1.0×10^5 and the angle of attack was 10 degrees. The initial condition of the velocity and pressure was given by an impulsive start from free stream conditions.

Figure 1 shows the streamline pattern of the result at non-dimensional time 1.2. The flow is attached to the surface of the wing. No oscillation is observed on the leeside of the wing. Figure 2 shows the streamline pattern of the result at a non-dimensional time 2. The flow observed over the leeside of the wing is oscillating in the region from the center of the wing to downward. The wavelength of the oscillation was calculated by measuring the length between each center of the vortex. The wavelength was approximately 0.1. This oscillation is observed at the beginning of the simulation and appears earlier than other types of oscillation. Therefore, it is considered that this oscillation is excited by the linear instability of the flow. Then, the stability analysis of the flowfield is carried out. The result of the numerical simulation at non-dimensional time 1.2 is selected as a basic flow. We focused on the region from the leading edge to 90% chord length of the leeside of the wing (see Fig.3). The stability of the flow in this region is calculated.

Figure 4 shows the frequency and the amplification factor of the mode which is obtained by the stability analysis. One of the characteristics of the approximate eigensystem analysis used in this study is that the approximation error of a mode is small if the amplification factor is large. Then, we focus on those modes whose amplification factors are large, and discuss those results.

The mode whose amplification factor is the largest is a non-oscillatory mode. The velocity disturbances of the mode at every grid points are plotted by arrow and shown in Fig.5.

At the boundary of the computational domain, the magnitude of the velocity disturbances is not small and that oscillates for the radial direction. From the result of the numerical simulation of flow (see Fig.2), no oscillation was observed in this position. Therefore, this mode is considered to be caused by some numerical reason. At the boundary of the computational domain, zero-order extrapolation is posed for the disturbance of the velocity and pressure. The boundary of the perturbation equations exists inside the computational domain which is used for the calculation of the basic flow. However, no oscillation is observed in the result of the numerical simulation of flow which was shown in Fig.2. Therefore, this mode is regarded as a non-physical mode. This kind of mode will be obtained when we analyze the stability of flow by calculating only the domain which is contained in the domain for the basic flow.

Figure 6 shows the mode whose amplification factor is the largest among the oscillatory mode. Since the amplification factor of this mode is positive, this mode will be amplified over time. The flow begins to oscillate according to the growth of this mode. Considering the superposition of this mode on the basic flow, it is anticipated that the configuration of the flow resembles to the oscillatory flow shown in Fig.2. The transition

from the flow shown in Fig.1 to the flow shown in Fig.2 is caused by the growth of the most unstable oscillatory mode which is shown in Fig.6.

3.2 $Re = 2.0 \times 10^5$ Case

To investigate the influence of the Reynolds number to the result of the stability analysis, the same procedure is carried out in the case that the Reynolds number is 2.0×10^5. The initial condition was given by an impulsive start. Figure 7 shows the streamline pattern of the result at non-dimensional time 1.2. The flow is attached to the surface of the wing and no oscillation is observed over the wing. Figure 8 shows the streamline pattern of the result at non-dimensional time 2. The flow is oscillating in the region from the center of the wing to downward on the leeside of the wing. The wavelength of the oscillation calculated by measuring the length between each center of the vortex is approximately 0.09. This value is a bit smaller than that of $Re = 1.0 \times 10^5$.

We focused on the region shown in Fig.3 and the stability of the flowfield at non-dimensional time 1.2 (see Fig.7) is calculated.

Figure 9 presents the frequency and the amplification factor of the mode which is obtained by the stability analysis. From the consideration of the result at $Re = 1.0 \times 10^5$, the mode was determined as a non-physical mode.

Figure 10 shows the mode whose amplification factor is the largest among the oscillatory mode. Since the amplification factor is positive, the flow begins to oscillate according to the advance of time. Considering the superposition of this mode on the basic flow, it is anticipated that the configuration of the flow resembles to the oscillatory flow shown in Fig.8. The growth of the mode shown in Fig.10 causes the transition from Fig.7 to Fig.8.

3.3 Comparisons with the Kelvin-Helmholtz Instability

To confirm the validity of the results calculated by the stability analysis, local stability analysis known as Kelvin-Helmholtz instability is applied to the velocity profile of the basic flow. The wave length and period of the most amplified mode is compared. In the previous study[12], the frequency of the oscillation observed in the laminar separation bubble was compared with the frequency of Kelvin-Helmholtz instability[13]. These results were in good agreement with each other. For the confirmation of this study, the frequency of the most amplified oscillatory mode is compared with that of Kelvin-Helmholtz instability[13]. The frequency was evaluated by Rayleigh equation which is a local stability analysis method of inviscid parallel flow. The velocity profile of the basic flow was approximated as:

$$U(y) = 0.5[1 + \tanh y].$$

As the stream function of disturbance ψ satisfy

$$\psi(x, y, t) = \Re[\phi(y) \exp\{i(\alpha x - \beta t)\}],$$

the frequency of the oscillation is calculated as $\beta / 2\pi$. The amplification factor of the oscillatory mode becomes the largest when β=0.206692.

The center of the region where the velocity disturbances exist in Fig.6 and Fig.10 is estimated at 60% of chord length. The velocity profile of this place is substituted to the result of the local stability analysis.

The velocity profile at 60% of chord length is shown in Fig.11. Figure 11(a) and Figure 11(b) is the result of the case $Re = 1.0 \times 10^5$ and $Re = 2.0 \times 10^5$, respectively. The horizontal axis shows the components of the velocity that is parallel to the surface of the wing. The vertical axis shows the distance normal to the surface of the wing. This profile is similar to the configuration of $U = \tanh(y)$. $U = \tanh(y)$ is modified as $U = a + b \tanh(y / c)$ and the best value of variables a, b, and c are found. The profile of $U = a + b \tanh(y / c)$ shown by dash line in Fig.11 agrees with the velocity profile.

The value of the frequency and the wave length calculated by our results and reference [13] is shown in Table 1. The order of those values is same. But those values are not exactly consistent. It should be pointed out that there is

a difference between local stability analysis of parallel inviscid flow and non-local stability analysis which treats a certain region of the viscid flowfield. If we take account of such difference, we can conclude that the value of the frequency and the wave length calculated by our results and reference[13] is almost the same. This result suggests that the method of stability analysis used in this study demonstrates reasonable results.

In the flow around a wing, several kinds of oscillatory phenomena are observed, for example, the oscillation of the wake[14], the high frequency oscillation of the laminar separation bubble and the low frequency oscillation in a stall angle of attack condition[15]. Future study will focus on such oscillatory phenomena. By applying our method and modifying the method furthermore, these oscillatory modes of such phenomena may be obtained. Those results will explain the mechanism of the oscillatory phenomena.

4. Conclusion

The method of the global stability analysis in a certain domain of the flowfield using the linear perturbation equation is applied for the flow around a NACA0012 airfoil.

The non-oscillatory flow observed at the beginning of the calculation is used as a basic flow for the stability analysis. We focused on the upper domain of the wing and the stability analysis of the region is numerically solved.

To investigate the effect of the viscosity, two cases of the Reynolds number, Re=1.0×10^5 and Re=2.0×10^5, were analyzed. In both case, the value of the frequency and the wavelength is almost the same.

Those results are compared with the local stability analysis. The order of the frequency and the wavelength is consistent with that of Kelvin-Helmholtz instability. Our method of the stability analysis is considered to calculate reasonable results.

References

[1] Natarajan R & Acrivos A. The instability of the steady flow past spheres and disks. *J. Fluid Mech.*, Vol. 254, pp 323-344, 1993.

[2] Tezuka A & Suzuki K. Global Stability Analysis of Flow Around an Ellipsoid at Angle of Attack. AIAA Paper, *33rd AIAA Fluid Dynamics Conference and Exhibit*, Orlando, 2003-4142

[3] Tezuka A & Suzuki K. The global stability analysis of steady flow around a blunted cylinder. *Proc. 4th Asia Workshop CFD*, Tokyo, pp 89-94, 2003.

[4] Chiba S. Global stability analysis of incompressible viscous flow. *J. Japan Soc. CFD*, Vol. 7, No. 1, pp 20-48, 1998. (in Japanese)

[5] Tezuka A. The global stability analysis based on the linear perturbation equation of incompressible flow and the approximate eigensystem analysis. *Proc. 35th Fluid Dyn. Conf.*, Kyoto, pp 217-220, 2003. (in Japanese)

[6] Dovgal AV, Kozlov VV & MichalkeA. Laminar boundary layer separation: instability and associated phenomena. *Prog. Aerospace Sci.*, Vol. 30, pp 61-94, 1994.

[7] Eriksson LE & Rizzi A. Computer-aided analysis of the convergence to steady state of discrete approximations to the euler equations. *J. Comp. Phys.*, Vol. 57, No. 1, pp 90-128, 1985.

[8] Arnoldi WE. The principle of minimized iterations in the solution of the matrix eigenvalue problem. *Quart. Appl. Math.*, Vol. 9, pp 17-29, 1951.

[9] Harlow FH & Welch JE. Numerical calculation of time-dependent viscous incompressible flow of fluid with free surface. *Phys. Fluids*, Vol. 8, pp 2182-2189, 1965.

[10] Greenspan D. Numerical Studies of Prototype Cavity Flow Problems. *Comput. J.*, Vol. 12, pp 89-94, 1969.

[11] Tezuka A. Stability analysis of a certain domain of flowfiled based on the linear perturbation equation and the approximate eigensystem analysis. *Proc. 17th CFD Sympo.*, Tokyo, pp 124, 2003. (in Japanese)

[12] Rinoie K & Sato J. Experiments on transition process of laminar separation bubble on airfoil. *J. Jpn. Soc. Aero. Space Sci.*, Vol. 38, No. 438, pp 352-361, 1990. (in Japanese)

[13] Michalke A. On spatially growing disturbances in an inviscid shear layer. *J. Fluid Mech.*, Vol. 23, No. 3, pp 521-544, 1965.

[14] Brooks TF & Schlinker RH. Progress in rotor broadband noise research. *Vertica*, Vol. 7, No. 4, pp 287-307, 1983.

[15] Zaman K, Mckinzie DJ & Rumsey CL. A natural low-frequency oscillation of the flow over an airfoil near stalling conditions. *J. Fluid Mech.*, Vol. 202, pp 403-442, 1989.

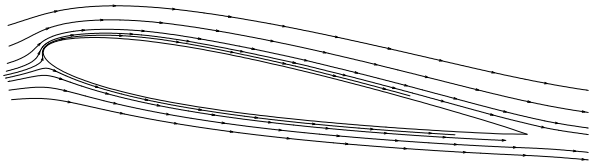

Fig. 1. Streamline at t=1.2 (Re=1.0×10^5)

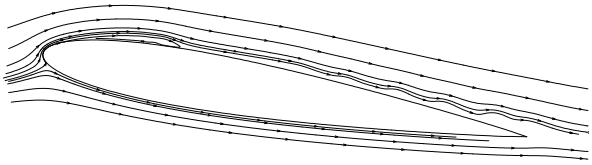

Fig. 2. Streamline at t=2 (Re=1.0×10^5)

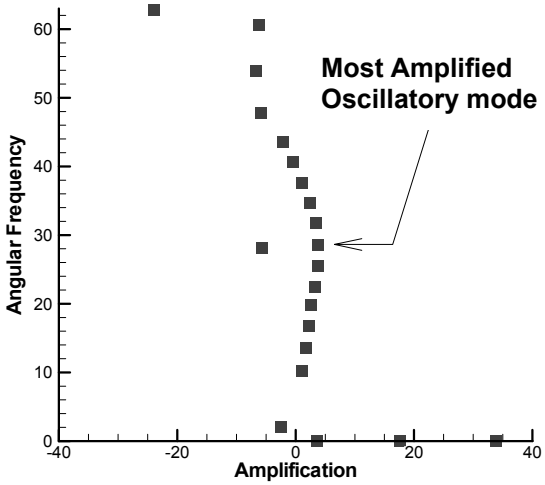

Fig. 4. Amplification factor and angular frequency of modes (Re=1.0×10^5)

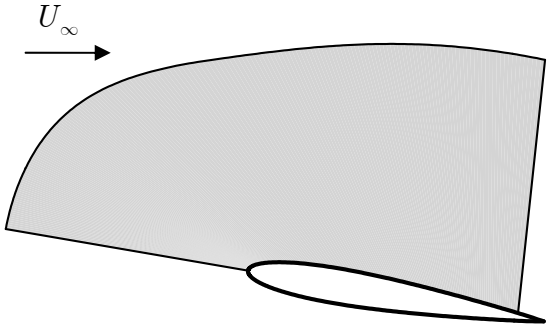

Fig. 3. Computational domain used for the stability analysis

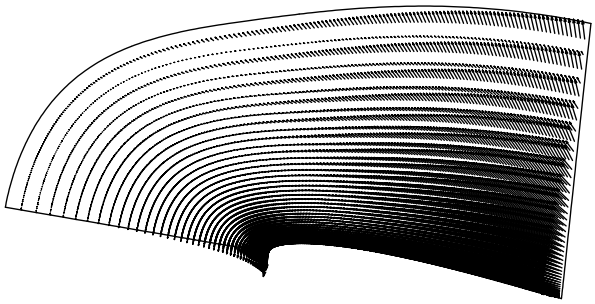

Fig. 5. Most amplified mode (Re=1.0×10^5)

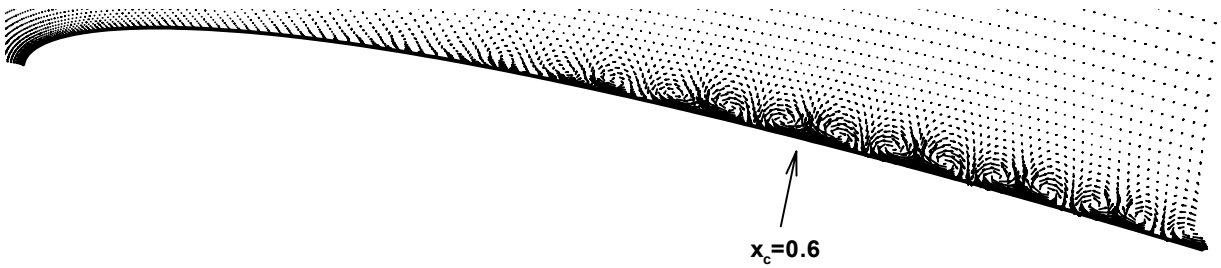

Fig. 6. Velocity disturbances of the most amplified oscillatory mode (Re=1.0×10^5)

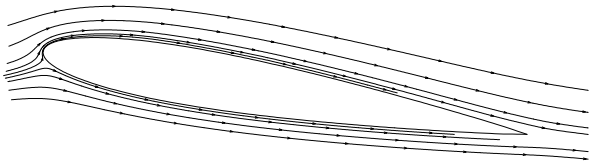

Fig. 7. Streamline at t=1.2 (Re=2.0×10^5)

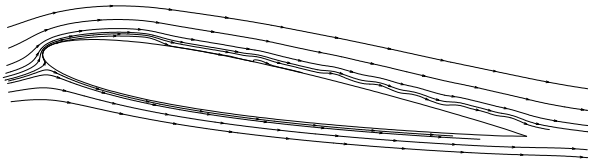

Fig. 8. Streamline at t=2 (Re=2.0×10^5)

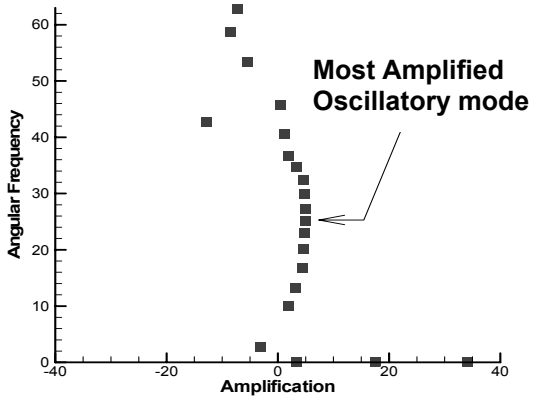

Fig. 9. Amplification factor and angular frequency of modes (Re=2.0×10^5)

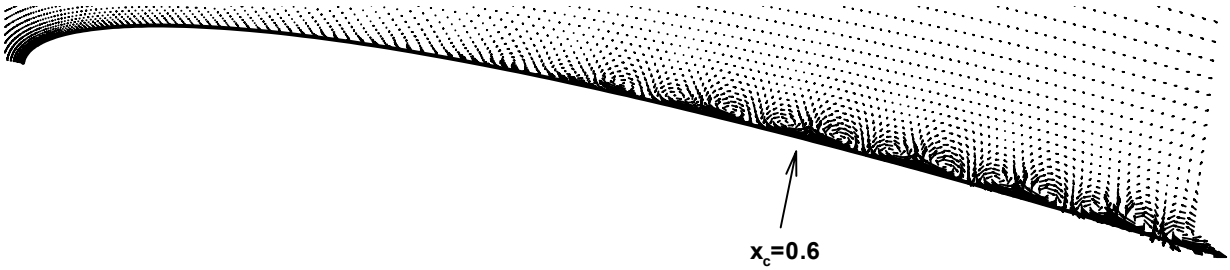

Fig. 10. Velocity disturbances of the most amplified oscillatory mode (Re=2.0×10^5)

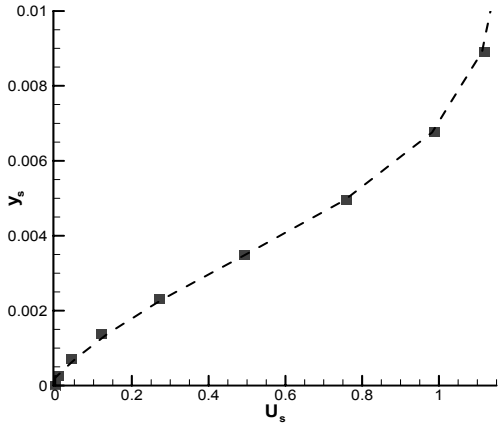

(a) Re=1.0×10^5 case

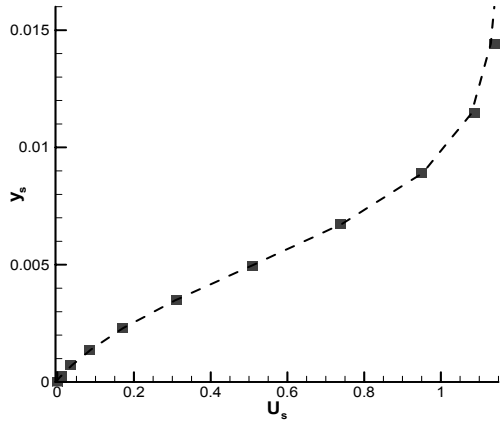

(b) Re=2.0×10^5 case

Fig. 11. Velocity profile at 60% chord length

Table l. Comparison of this result with the Kelvin-Helmholtz instability

(a) Re=1.0×10^5 Case

	wave length	period
Present study	0.082	0.25
Linear stability analysis	0.073	0.22

(b) Re=2.0×10^5 Case

	wave length	period
Present study	0.082	0.25
Linear stability analysis	0.058	0.16